Research Article

Hongbo Tang*, Jian Zhou, Shengkui Zhong, Yuchang Su, Qunwei Shu and Lihua Xiao*

Preparation, optical properties, and thermal stability of polyvinyl butyral composite films containing core (lanthanum hexaboride)–shell (titanium dioxide)-structured nanoparticles

https://doi.org/10.1515/secm-2021-0055
received April 06, 2021; accepted September 29, 2021

Abstract: Nano-sized lanthanum hexaboride (LaB_6)@titanium dioxide (TiO_2) particles with a core–shell structure has been successfully synthesized via a simple sol–gel method. LaB_6@TiO_2 particles were used as filler in polyvinyl butyral (PVB) matrix and performance of the TiO_2 shell was evaluated. The core–shell nanoparticles were characterized for morphology and structure properties. X-ray diffraction and transmission electron microscope testing results confirm the formation of LaB_6–TiO_2 core–shell structure. In composite film, LaB_6 improved the thermo-decomposing temperature of PVB matrix from 369.2 to 372.8°C, while the same amount of LaB_6@TiO_2 further increased the temperature to 381.0°C. In addition, TiO_2 shell redshifted the maximum transmittance of the film from 605 to 669 nm in the visible region. In the near infrared region, its absorption peak shifted from 1,466 to 1,476 nm. This result will be helpful for the development of transparent and thermal insulating materials.

Keywords: LaB_6@TiO_2 particles, optical properties, heat insulating materials, thermal stability, core–shell structure

*** Corresponding author: Hongbo Tang,** Key Laboratory of Jiangxi University for Applied Chemistry and Chemical Biology, Yichun University, Yichun 336000, People's Republic of China, e-mail: thblzj@126.com
*** Corresponding author: Lihua Xiao,** School of Marine Science and Technology, Hainan Tropical Ocean University, Hainan 572000, People's Republic of China; School of Materials and Energy Engineering, Guizhou Institute of Technology, Guiyang 550003, People's Republic of China, e-mail: xiaolihua@git.edu.cn
Jian Zhou: Key Laboratory of Jiangxi University for Applied Chemistry and Chemical Biology, Yichun University, Yichun 336000, People's Republic of China
Shengkui Zhong: School of Marine Science and Technology, Hainan Tropical Ocean University, Hainan 572000, People's Republic of China
Yuchang Su: School of Materials Science and Engineering, Central South University, Changsha 410083, People's Republic of China
Qunwei Shu: School of Materials and Energy Engineering, Guizhou Institute of Technology, Guiyang 550003, People's Republic of China

1 Introduction

As a thermionic electron emitter material, LaB_6 is known for its excellent thermal stability, creep resistance, low work function, and so on. Up to now LaB_6 is found to possess higher electronic emissivity than other materials and therefore, it has been extensively applied in various areas, such as electron lithography, high resolution optical system, and coating film for resistor [1–4].

Surface plasmon resonance refers to collective oscillations of metallic electrons at the metal-dielectric interface. The metal-like plasmonic material lanthanum hexaboride (LaB_6) exhibits strong surface plasmon resonance absorption in the near infrared (NIR) region after being reduced to the nanoscale [5,6]. It indicates that LaB_6 absorbs the NIR light, while maintaining high transparency in visible region. Hence, LaB_6 acts as effective component in functional materials to impair heat transmission [7]. And now, different forms of the nanoparticles (NPs) like filler or coating of polymer films have found applications in glass curtain wall and automotive glass [8,9].

During the early 1990s, researchers prepared concentric multilayer semiconductor Nps in order to improve materials' properties. Since then, materials with a core–shell structure have attracted much attention [10–12]. This kind of materials could be synthesized by combining many components to form various cores and shells. These nanoscaled particles have many advantages over single components, such as wider applicability, better tunability, and higher sensitivity. Indeed, extensive research has been conducted on these materials. Kim et al. found

that Ag/TiO_2 core–shell nanowires imparted exquisite resistance switching behavior to flexible, composite, and the ultra-thin shell in NPs and enhanced thermal stability of Ag core, while effectively blocking recombination of excitons [13]. Thus, this material was efficient in the disinfection of water under solar light irradiation due to distinctive surface plasmon resonance and electron charge transfer [14]. Controllable rutile titanium dioxide (TiO_2) shell in anatase@rutile core@shell TiO_2 nanosheets improved ethanol sensing performances [15]. Obviously, TiO_2 shell has attracted a great deal of interest in many fields due to its excellent chemical stability, photochemical activity, antibacterial activity, and so on [16–19].

More importantly, TiO_2 helps LaB_6 NPs distribute uniformly in polyvinyl butyral (PVB) due to electrostatic attraction formed at the interfaces between TiO_2 and LaB_6 [20]. So we expected to integrate LaB_6 core and TiO_2 shell to investigate how the shell would act in the core–shell structure and relevant properties. In the present study, PVB-based hybrid nanocomposite films were prepared by using core–shell structured LaB_6@TiO_2 NPs as fillers. The effect of the core–shell NPs on optical and thermal properties of the nanocomposite films will be introduced in this article.

2 Experimental methods

2.1 Materials

LaB_6 particles with diameter of 20–50 nm were provided by Ronghua Technology Co. (China). Tetrabutyl orthotitanate, silane coupling agent KH570, ammonium hydroxide (28–30 wt%), PVB (average molecular weight = 35,000–45,000 g/mol), dodecylbenzenesulfonic acid, ethanol, and ammonia were selected from Aladdin Chemical Co. (China). Deionized water was used throughout.

2.2 Preparation of core–shell LaB_6@TiO_2 NPs

According to Chen et al. research [21], LaB_6 NPs need to be pretreated with an anionic surfactant dodecylbenzenesulfonic acid to achieve a stable dispersion of LaB_6 in ethanol. In brief, LaB_6 particles were mixed with ethanol solution of dodecylbenzenesulfonic acid (0.05 wt%), and the content of LaB_6 NPs was fixed at 1 wt%. Then, the mixture was stirred for a few minutes until a navy blue suspension was obtained. In order to achieve better homogenization, it was subsequently milled in a planetary ball mill for 24 h.

A sol–gel-assisted hydrothermal method elaborated elsewhere [22] was used for preparation of LaB_6@TiO_2 NPs. At first, 20 mL of the navy blue suspension, 2 mL of $NH_3{\cdot}H_2O$, and 2 mL of tetrabutyl orthotitanate were added to 100 mL of ethanol-water (with volume ratio of ethanol/water = 9/1). Then, the obtained mixture was kept in a water bath at 40°C under vigorous stirring for 6 h. In this process, amorphous TiO_2 shells were formed on surfaces of LaB_6 NPs. Subsequently, a hydrothermal process was used to prepare LaB_6@TiO_2 NPs with anatase TiO_2 shells. The suspension was transferred into a Teflon-sealed autoclave and then placed in an oven at 160°C for 6 h. The products were collected by centrifugation and washed with distilled water and absolute ethanol several times.

2.3 Preparation of LaB_6@TiO_2-PVB and LaB_6-PVB nanocomposite films

Preparation of LaB_6@TiO_2-PVB composite films consisted of three steps. First, PVB powders were dissolved in ethanol via continuous stirring at 65°C for almost 1 h, and volume of ethanol was fixed at 50 mL throughout. Thus, ethanol solution of PVB was obtained. Second, LaB_6@TiO_2 particles and silane coupling agent KH570 were mixed in ethanol under vigorous stirring in an ultrasonic bath. KH570 aimed to promote the compatibility and dispersion of LaB_6@TiO_2 in PVB matrix. After complete dispersion, a stable navy blue suspension appeared. Finally, the suspension and an ethanol solution of PVB (10 wt%) were vigorously stirred at 65°C for 6 h (including 30 min of ultrasonic treatment). The as-obtained mixture was then cast onto slides by dip-coating method, and subsequently dried at 40°C for 24 h. After drying, films were removed from slides. Thickness of the films was fixed between 0.15 and 0.3 mm. A schematic diagram for fabrication of LaB_6@TiO_2 NPs and LaB_6@TiO_2-PVB nanocomposite films was presented in Figure 1. LaB_6-PVB films were produced when the fillers were LaB_6 NPs.

2.4 Measurements

Morphology of LaB_6@TiO_2 NPs was determined by Transmission electron microscope (FEI-TEM; Tecnai G2 F20

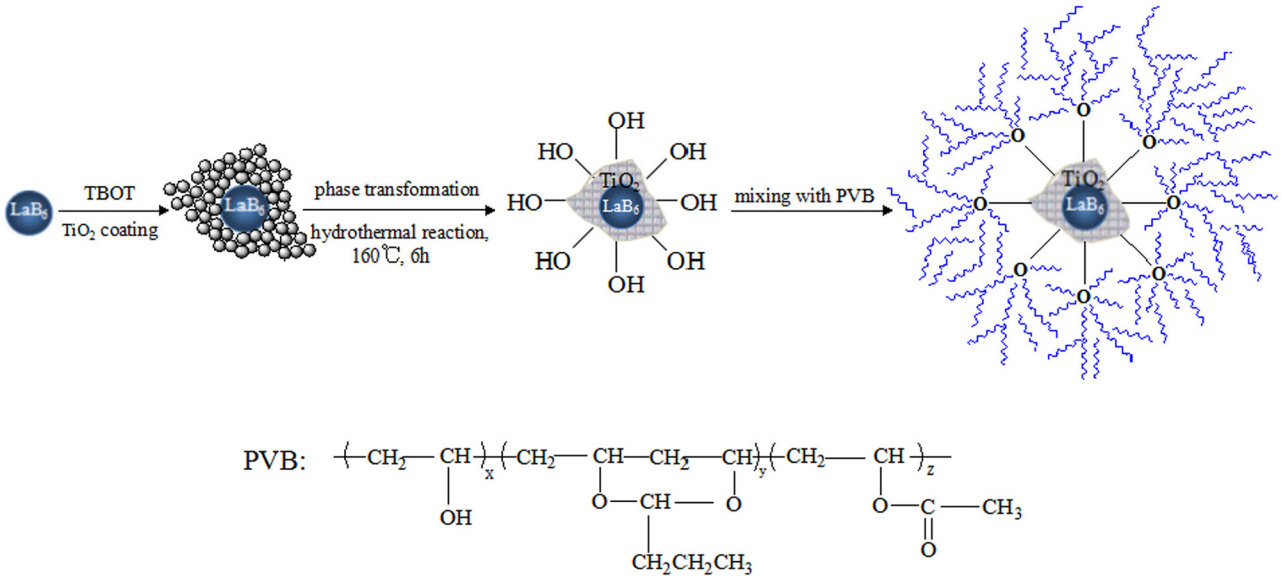

Figure 1: The schematic diagram of fabrication of LaB_6@TiO_2 NPs and LaB_6@TiO_2-PVB nanocomposite films.

S-TWIN) equipped with energy dispersive X-ray spectroscopy. For the TEM measurement, LaB_6@TiO_2 NPs were dispersed in ethanol and then transferred onto a copper grid covered with carbon film. XRD patterns of LaB_6, TiO_2, and LaB_6@TiO_2 NPs were recorded by D-MAX2500 (Rigaku) with Cu Kα radiation (λ = 0.1542 nm and step size = 0.02°) at a scanning rate of 8°/min in the 2θ range of 15–80°. Nicolet-6700 spectrophotometer (USA) with 4/cm resolution was used to measure the FT-IR spectra of PVB and nanocomposite films in the range of 4,000–400/cm.

The UV-Vis-NIR transmission spectra of 0.30 wt% LaB_6-PVB film and 0.30 wt% LaB_6@TiO_2-PVB nanocomposite films were detected by a UV-vis-NIR spectrophotometer (Japan, Shimadzu UV-3600) in a wavelength range of 380–2,000 nm. The neat PVB films were set as a blank background. Thermogravimetric findings (TGA) and differential scanning calorimeter (DSC) curves of neat PVB and nanocomposite films were recorded by a STA449C simultaneous thermal analyzer at a heating rate of 10°C/min from 25 to 700°C under N_2 atmosphere.

3 Results and discussion

3.1 XRD patterns

Figure 2 presents the XRD patterns of LaB_6, TiO_2, and LaB_6@TiO_2 NPs. The diffraction planes at 21.4°, 30.4° (strongest), 37.4°, 43.5°, and 49.0° were assigned to the (100), (110), (111) (200), and (210) planes of cubic LaB_6 (JCPDS No. 34-0427), respectively. TiO_2 prepared through the sol–gel-assisted hydrothermal method exhibited diffraction peaks at 25.4° (strongest), 37.0°, 37.8°, 38.6°, 48.1°, and 54.0° which were attributed to (101), (103), (004), (112), (200), and (105) crystal faces of anatase phase (JCPD No. 89-4921), respectively. Since LaB_6 NP was enveloped with TiO_2 shell by a sol–gel hydrothermal process, diffraction peaks of the core–shell structured particles were compatible with cubic LaB_6 and anatase TiO_2. In addition, no other diffractive peaks appear in the pattern. Neetu [23] and Liu et al. [24] also reported hydrothermal synthesis of anatase TiO_2 shell, and their XRD patterns are consistent with ours. It is concluded that

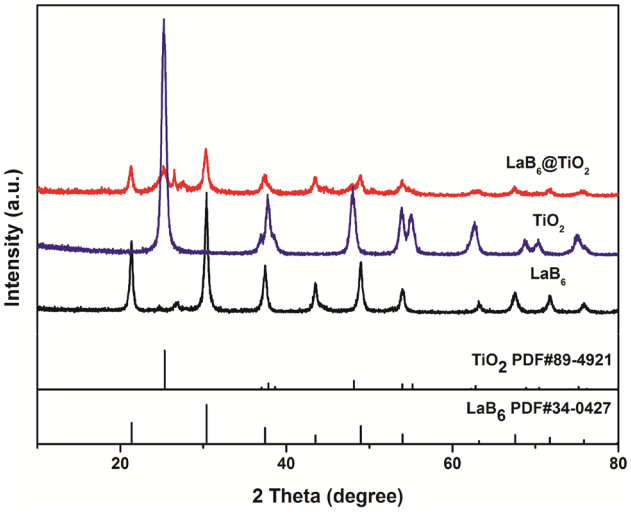

Figure 2: XRD patterns of LaB_6, TiO_2, and LaB_6@TiO_2 NPs.

the sol–gel-assisted hydrothermal method to prepare the $LaB_6@TiO_2$ NPs with high purity is feasible.

3.2 Morphology analysis

The size and structure of the core–shell-structured $LaB_6@TiO_2$ NPs is determined using TEM characterization technique and the images are shown in Figure 3. It is clearly visible in Figure 3a that many particles with an average diameter of 80 nm are aggregated and there is a shielding of core particles by the TiO_2 shell. Figure 3b presents an electron diffraction (ED) pattern of the $LaB_6@TiO_2$ NPs. The diffraction rings are attributed to (100) and (110) planes of LaB_6 (PDF#-34-0427) and (101) and (103) planes of TiO_2 (PDF#-89-4921), respectively. In order to detect the elements of the composite NPs, samples were analyzed by EDX, and the results are displayed

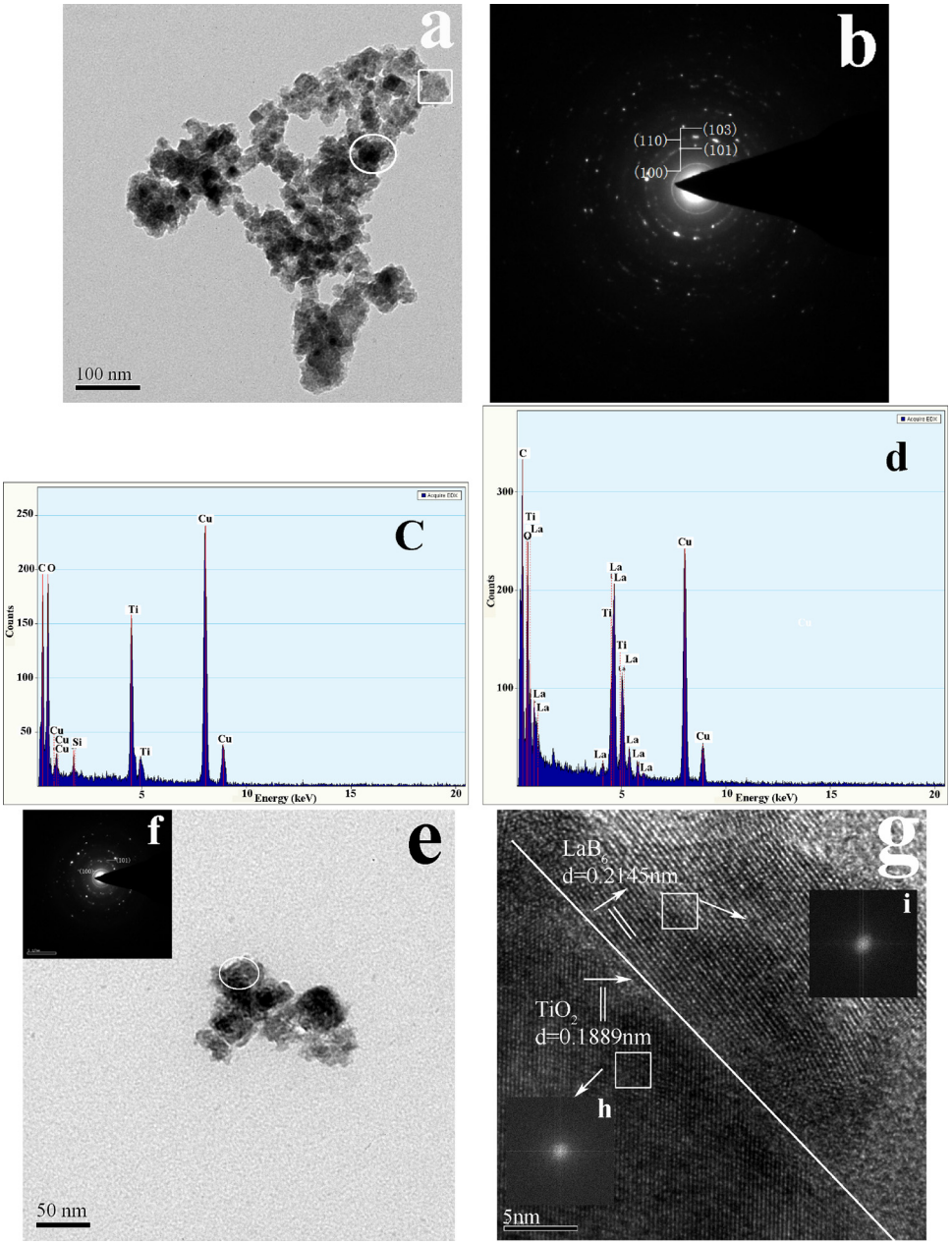

Figure 3: (a) TEM image and (b) electron diffractive spots of $LaB_6@TiO_2$ NPs. EDX results of (c) the square spot and (d) the circular spot in (a). (e) TEM image and (f) electron diffractive spots of a $LaB_6@TiO_2$ NP. (g) HRTEM image of $LaB_6@TiO_2$ NP, the insets (h) and (i) are FFT images of the core and the shell, respectively.

in Figure 3c and d, corresponding to spots marked by the square and the circle in Figure 3a, respectively. As shown in Figure 3c, Ti peaks which are attributable to TiO_2 shell formed in the sol–gel method are significantly distinguished from other peaks, and O peak is attributed to TiO_2 and residual dodecylbenzenesulfonic acid absorbed on surfaces of LaB_6@TiO_2 core–shell NPs. Besides, no La peaks are found. As compared to Figure 3c, La peaks in Figure 3d are apparently observed due to high content of LaB_6 at this spot. However, the light element boron does not present any peaks here due to its property, or the peaks may be overlapped by carbon's. In addition, Ti, C, and O elements were also detected. Two peaks at 8–9 keV are originated from the Cu substrate used for TEM detection. Combined with the TEM image in Figure 3a, it can be obtained that the NPs are only consisted of LaB_6 and TiO_2 without any other elements, which is in good agreement with the XRD findings; and the dark LaB_6 cores are surrounded by TiO_2 shell.

A high-resolution TEM image of a single LaB_6@TiO_2 NPs is presented in Figure 3e. The inner LaB_6 core is tightly surrounded by a loose TiO_2 layer, and the interface between the dark core and the translucent continuous shell is noticed. Most of the shells possess a thickness less than 5 nm, but a few of them are approximately 15 nm thick. Figure 3f (inset in Figure 3e) is an ED pattern of the section marked by a circle. To further demonstrate the detailed microstructure of the interface between the cores and shells, high-resolution TEM (HRTEM) and fast Fourier transmission (FFT) measurements were carried out, and data are displayed in Figure 3g. It is clearly displayed that the two different crystal growth directions which are perpendicular to their corresponding crystal planes exist, with a distinct boundary between them. The inter-planar spacing of around 0.2145 nm is attributed to the (200) plane of LaB_6 and the lattice spacing of approximately 0.1899 nm is ascribed to the (200) plane of TiO_2. Moreover, Figure 3h and i illustrates diffractive spots of anatase TiO_2 shell and crystalline LaB_6 core, respectively. These results further confirm that there are two different crystal forms in the LaB_6@TiO_2 NPs, coinciding with the results of the above XRD patterns.

3.3 FT-IR spectra

FT-IR spectra of the composites are exhibited in Figure 4. For the pure PVB films, the peaks at 1,700–1,600 and 3,700–3,100/cm are attributed to the stretching and bending vibrations of O–H in PVB matrix, ethanol, or H_2O left in the films. The peaks at 2,956 and 2,877/cm correspond to the

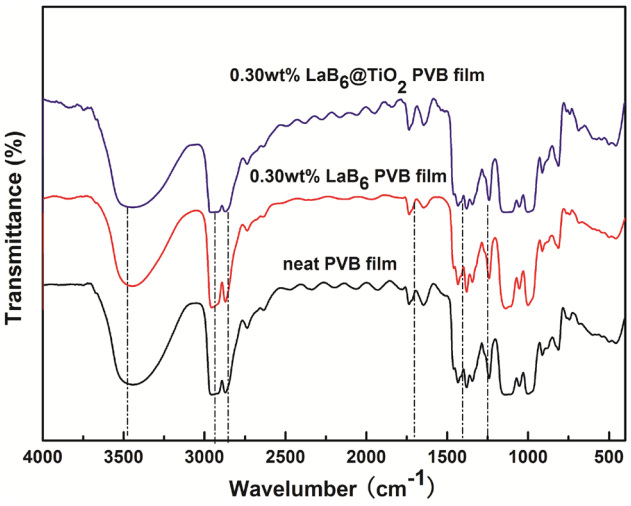

Figure 4: FT-IR spectra of the films.

stretching vibration of aliphatic C–H groups. The peaks at 1,435, 1,382, and 1,346/cm are attributed to the bending vibration of C–H groups. The peaks at 1,135 and 1,047/cm are originated from C–O–C–O–C stretching vibration of pentatomic and hexatomic cyclic acetal groups. The peaks at around 1,731/cm belong to the stretching vibration of C═O in acetate group. The peaks at 987 and 1,234/cm are assigned to –OH asymmetric stretching of polyvinyl alcohol [25]. For the LaB_6@TiO_2-PVB, the peaks at around 520/cm are characteristic peaks of TiO_2 crystals [20] and ascribable to the stretching vibration of Ti–O–Ti bonds in TiO_2 [26,27]. Tekin et al. [28] also observed Ti–O–Ti stretching vibration modes of anatase TiO_2 in a form of a broadband ranging from 647 to 830/cm.

These spectra are similar in appearance, and it may be attributed to low contents of solid particles in the composite films and their weak absorption in this region.

3.4 Thermal degradation characteristics

The thermodynamic stability of the films was investigated by means of DSC and TGA (Figure 5). As demonstrated by a TGA curve in Figure 5a, thermal degradation of neat PVB film included two steps. The first weight loss that occurred below 100°C may be resulted from water evaporation in the matrix, which was absorbed in the film due to Van der Waals force. The second weight loss that started at 250°C and finished at 400°C is probably attributed to the degradation of PVB matrix, and it exhibited a weight loss of 90.3%. However, it is obvious that PVB in LaB_6-PVB and LaB_6@TiO_2-PVB films degraded at higher temperatures. Especially for LaB_6@TiO_2-PVB

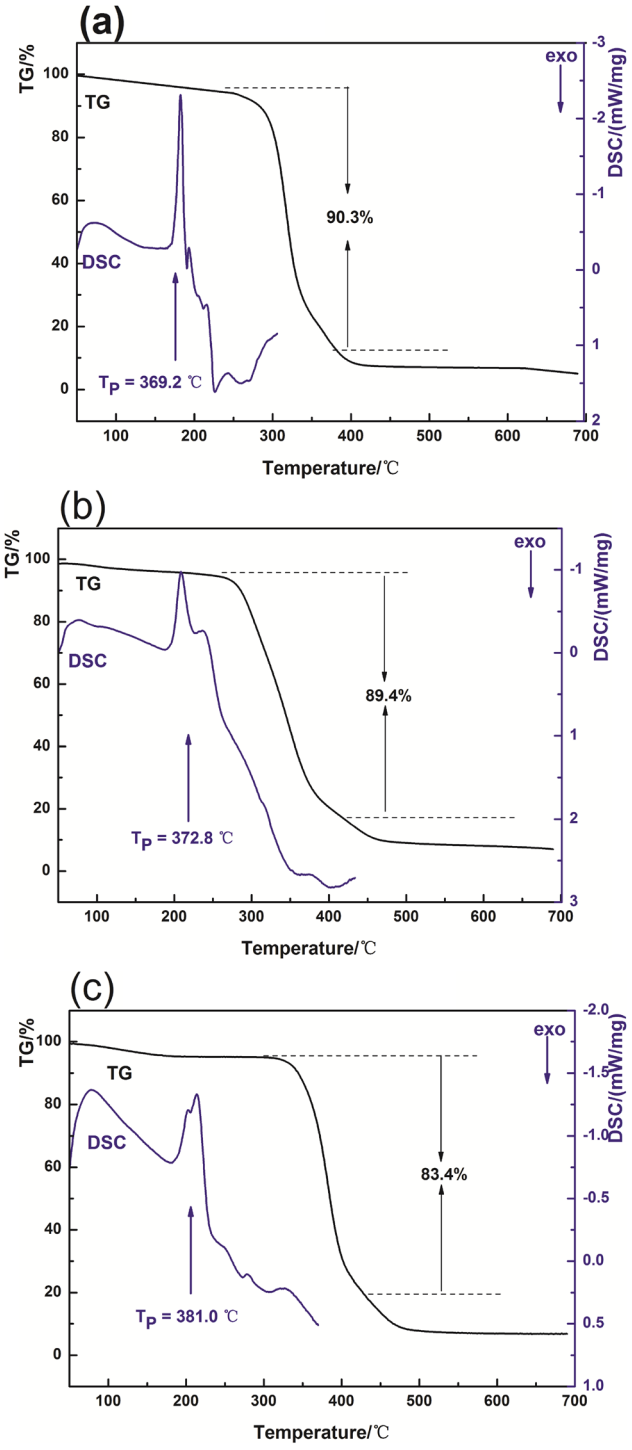

Figure 5: TGA and DSC thermograms of the films: (a) neat PVB, (b) LaB_6-PVB, and (c) LaB_6@TiO_2-PVB.

nanocomposite films, it happened at around 320°C. Additionally, LaB_6-PVB and LaB_6@TiO_2-PVB nanocomposite films presented weight loss of 89.4% (Figure 5b) and 83.4% (Figure 5c), respectively. As a comparison, 0.3 wt% LaB_6@TiO_2-PVB film is not vulnerable to heat.

Endothermic peaks at 369.2°C (Figures 5a), 372.8°C (Figure 5b), and 381.0°C (Figure 5c) are apparently noticed in the DSC curves of neat PVB, LaB_6-PVB, and LaB_6@TiO_2-PVB nanocomposite films, respectively, and they might be originated from degradation of PVB matrix. In addition, when LaB_6@TiO_2 NPs were added into neat PVB, the decomposition temperature of the matrix almost improved from 369.2 to 381.0°C, indicating an enhancement of thermal properties of the nanocomposite films. This phenomenon should be ascribed to the strong hydrogen bonding effect between the polar hydroxyl groups of PVB and the oxygen atoms of LaB_6@TiO_2 NPs. Similar reports have been presented by Hemdana et al. [12] and Mallakpour and Dinari [26].

3.5 UV-Vis-NIR spectra

Transmission spectra of 0.30 wt% LaB_6-PVB and 0.30 wt% LaB_6@TiO_2-PVB nanocomposite films in Figure 6 were measured in a wavelength region between 380 and 2,000 nm. Both samples show high transmittance in visible region (380–780 nm), and strong absorption peaks in NIR region (780–1,500 nm), and their transmittance curves in the spectra are similar in appearance. Additionally, transmittance spectra of LaB_6-PVB and LaB_6@TiO_2-PVB nanocomposite films are almost the same with a maximum absorption in the region of 1,000–1,500 nm. In contrast, LaB_6@TiO_2-PVB nanocomposite films illustrated better transmittance in visible region.

The peak transmittance of LaB_6-PVB and LaB_6@TiO_2-PVB film were located at 605 and 669 nm, respectively.

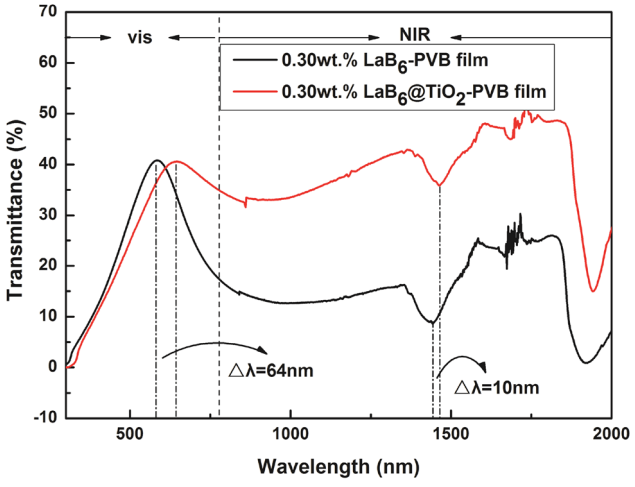

Figure 6: Transmittance spectra of composite films.

It means that an anatase TiO_2 shell enables the peak transmittance to redshift for around 64 nm in visible region, and the absorption peak in NIR region to shift slightly from 1,466 to 1,476 nm. It might be attributed to enlarged diameter of LaB_6@TiO_2 NPs by TiO_2 shell. As has been reported in a previous research, enlarged diameter of a core–shell structure enabled absorption peak and transmission peak to redshift [12]. Thereby, it provides us a promising method to tune the wavelength range of the visible light transmission without any effect on the absorption of the NIR light.

To the best of our knowledge, films with high transmittance in the visible region and low thermal insulating properties have great application potential in automobile glasses. Based on the above results, the LaB_6@TiO_2-PVB nanocomposite films could fulfill these two requirements and therefore, would be a potential candidate for transparent heat-insulated materials in some applications.

4 Conclusion

LaB_6@TiO_2 NPs with a core–shell structure have been synthesized via a sol–gel-assisted hydrothermal method. XRD characterization shows that the NPs are composed of cubic LaB_6 and anatase TiO_2. TEM results confirm that the NP is composed of a cubic LaB_6 core and an anatase TiO_2 shell. FT-IR and TGA analyses illustrate that the thermal stability of the composite was enhanced by the TiO_2 shell due to the interaction between the NPs and PVB matrix. In LaB_6@TiO_2-PVB nanocomposite films, an anatase TiO_2 shell apparently expands the wavelength range of the visible light transmission of the composite films. This work provides us a comparatively simple method to synthesis LaB_6@TiO_2 NPs and a feasible way to produce composite films with high light transmittance and high thermal insulation.

Funding information: This work is financially supported by the National Natural Science Foundation of China (No. 51776046), the Natural Science Foundation of Jiangxi Province (Grant No. 20161BAB216097), and the Foundation of Jiangxi Provincial Education Department (Grant Nos. GJJ161022 and GJJ161035), the Science and Technology Project of Guizhou Province ([2019]1133) and Youth Science and Technology Talent Development Fund in Guizhou Provincial Department of Education ([2018]250).

Author contributions: Hongbo Tang and Jian Zhou conducted experiments and analyzed data and then prepared all the figures and wrote the main manuscript. Lihua Xiao and Yuchang Su oversaw the project and guided the writing of the manuscript. The manuscript was reviewed by all the authors.

Conflict of interest: Authors state no conflict of interest.

References

[1] Torgasin K, Morita K, Zen H, Masuda K, Bakr M, Nagasaki K, et al. Study on anomalous photoemission of LaB_6 at high temperatures. Phys Scr. 2019;94:075701.
[2] Lai BH, Chen DH. Vancomycin-modified LaB_6@SiO_2/Fe_3O_4 composite nanoparticles for near-infrared photothermal ablation of bacteria. Acta Biomater. 2013;9:7573–9.
[3] Zhang H, Tang J, Zhang Q, Zhao GP, Yang G, Zhang J, et al. Field emission of electrons from single LaB_6 nanowires. Adv Mater. 2006;18:87–91.
[4] Bogomol I, Nishimura T, Vasylkiv O, Sakka Y, Loboda P. High-temperature strength of directionally reinforced LaB_6-TiB_2 composite. J Alloy Compd. 2010;505:130–4.
[5] Schelm S, Smith GB, Garrett PD, Fisher WK. Tuning the surface-plasmon resonance in nanoparticles for glazing applications. J Appl Phys. 2005;97:124314.
[6] Takeda H, Kuno H, Adachi K. Solar control dispersions and coatings with rare-earth hexaboride nanoparticles. J Am Ceram Soc. 2008;91:2897–902.
[7] Smith GB, Deller CA, Swift PD, Gentle A, Garrett PD, Fisher WK. Nanoparticle-doped polymer foils for use in solar control glazing. J Nanopart Res. 2002;4:157–65.
[8] Yuan YF, Zhang L, Hu LJ, Wang W, Min GG. Size effect of added LaB_6 particles on optical properties of LaB_6/Polymer composites. J Solid State Chem. 2011;184:3364–7.
[9] Adachi K, Miratsu M. Absorption and scattering of near-infrared light by dispersed lanthanum hexaboride nanoparticles for solar control filters. J Mater Res. 2010;25:510–21.
[10] Tang J, Salunkhe RR, Liu J, Torad NL, Imura M, Furukawa S. Thermal conversion of core–shell metal-organic frameworks: a new method for selectively functionalized nanoporous hybrid carbon. J Am Chem Soc. 2015;137:1572–80.
[11] Zhu H, Zhang JF, Yanzhang RP, Du ML, Wang QF, Gao GH, et al. When cubic cobalt sulfide meets layered molybdenum disulfide: a core–shell system toward synergetic electrocatalytic water splitting. Adv Mater. 2015;27:4752–9.
[12] Hemdana I, Mahdouani M, Bourguiga R. Investigation of the third-order nonlinear optical susceptibilities associated with intersubband transitions in CdSe/ZnS/SiO_2 core/shell/shell quantum dot. Superlattice Microst. 2013;60:336–48.
[13] Kim Y, Jeon W, Kim M, Park JH, Hwang CS, Lee SS. Modulated filamentary conduction of Ag/TiO_2 core–shell nanowires to impart extremely sustained resistance switching behavior in a flexible composite. Appl Mater Today. 2020;19:100569–77.
[14] Sreeja S, Shetty KV. Photocatalytic water disinfection under solar irradiation by Ag@TiO_2 core–shell structured nanoparticles. Sol Energy. 2017;157:236–43.

[15] Zhang J, Chen C, Lu H, Leng D, Li G, Liu Y, et al. Construction of anatase@rutile core@shell TiO_2 nanosheets with controllable shell layer thicknesses for enhanced ethanol sensing. Sens Actuators: B Chem. 2020;325:128815–26.
[16] Jeong K, Deshmukh PR, Park J, Sohn Y, Shin WG. ZnO-TiO_2 core–shell nanowires: a sustainable photoanode for enhanced photoelectrochemical water splitting. ACS Sustain Chem Eng. 2018;6:6518–26.
[17] Shin D, Shin J, Yeo T, Hwang H, Park S, Choi W. Scalable synthesis of triple-core–shell nanostructures of TiO_2@MnO_2@C for high performance supercapacitors using structure-guided combustion waves. Small. 2018;14:1703755.
[18] El-Maghrabi HH, Barhoum A, Nada AA, Moustafa YM, Seliman SM, Youssef AM, et al. Synthesis of mesoporous core–shell CdS@TiO_2 (0D and 1D) photocatalysts for solar-driven hydrogen fuel production. J Photoch Photobio A. 2018;351:261–70.
[19] Wang YY, Yang WJ, Chen XJ, Wang J, Zhu YF. Photocatalytic activity enhancement of core–shell structure g-C_3N_4@TiO_2 via controlled ultrathin g-C_3N_4 layer. Appl Catal B-Environ. 2018;220:337–47.
[20] Ruan WK, Xie MB, Peng LZ, Liu CQ. Preparation and properties of the film of PVB resin modified with nano-TiO_2-doped LaB_6. Mater Today Chem. 2020;17:100283–9.
[21] Chen CJ, Chen DH. Preparation of LaB_6 nanoparticles as a novel and effective near-infrared photothermal conversion material. Chem Eng J. 2012;180:337–42.
[22] Zakaria SY, Samadi S, Cordshooli GA. Synthesis and characterization of zirconium (IV) and vanadium (III) doped CeO_2/TiO_2 core/shell nanostructures as a gas sensor. Sens Actuators A. 2021;318:112226.
[23] Neetu, Singh S, Srivastava P, Bahadur L. Hydrothermal synthesized Nd-doped TiO_2 with Anatase and Brookite phases as highly improved photoanode for dye-sensitized solar cell. Sol Energy. 2020;208:173–81.
[24] Liu X, Chen Y, Chen T, Liu Y, Han G, Xu G. One-pot hydrothermal synthesis of the dual-phase anatase/TiO_2-B nanoparticles with $K_2Ti_6O_{13}$ nanofibers for enhanced photocatalysis. Mater Lett. 2021;302:130333.
[25] Qin XX, Cheng ZL. Application of ionic liquids as a catalyst in the synthesis of polyvinyl butyral (PVB) polymer. Chin Chem Lett. 2016;27:145–8.
[26] Mallakpour S, Dinari M. The synergetic effect of chiral organoclay and surface modified-Al_2O_3 nanoparticles on thermal and physical properties of poly(vinyl alcohol) based nanocomposite films. Prog Org Coat. 2013;76:263–8.
[27] Liu C, Yang D, Jiao Y, Tian Y, Wang Y, Jiang Z. Biomimetic synthesis of TiO_2-SiO_2-Ag nanocomposites with enhanced visible-light photocatalytic activity. ACS Appl Mater Interfaces. 2013;5:3824–32.
[28] Tekin D, Birhan D, Kiziltas H. Thermal, photocatalytic, and antibacterial properties of calcinated nano-TiO_2/polymer composites. Mater Chem Phys. 2020;251:123067–72.